Integrated Genomic and Proteomic Analyses of a Systematically Perturbed Metabolic Network

Trey Ideker, *et al.*

Science **292**, 929 (2001);
DOI: 10.1126/science.292.5518.929

AMPARs in Bergmann glia are necessary for preventing surplus CFs from producing synapses onto single Purkinje cells.

Conversion of Ca^{2+}-permeable AMPARs into Ca^{2+}-impermeable receptors in Bergmann glia elicited morphological changes in fine glial processes wrapping Purkinje cell synapses, prolonged the kinetics of glutamatergic synaptic transmission, and caused multiple innervation of Purkinje cells by CFs. Thus, the morphology of glial processes and the synaptic activities would be interdependent. The Ca^{2+}-permeable AMPARs in glial cells probably play key roles in such interactions between glia and glutamatergic synapses.

References and Notes

1. P. H. Seeburg, *Trends Neurosci.* **16**, 359 (1993).
2. M. Hollmann, S. Heinemann, *Annu. Rev. Neurosci.* **17**, 31 (1994).
3. C. Steinhauser, V. Gallo, *Trends Neurosci.* **19**, 339 (1996).
4. M. Hollmann, M. Hartley, S. Heinemann, *Science* **252**, 851 (1991).
5. N. Burnashev, H. Monyer, P. H. Seeburg, B. Sakmann, *Neuron* **8**, 189 (1992).
6. K. Keinänen *et al.*, *Science* **249**, 556 (1990).
7. T. Müller, T. Möller, T. Berger, J. Schnitzer, H. Kettenmann, *Science* **256**, 1563 (1992).
8. N. Burnashev *et al.*, *Science* **256**, 1566 (1992).
9. For the methods used, see the supplementary information on *Science* Online at www.sciencemag.org/cgi/content/full/292/5518/926/DC1.
10. K. A. Yamada, C. M. Tang, *J. Neurosci.* **13**, 3904 (1993).
11. K. M. Partin, M. W. Fleck, M. L. Mayer, *J. Neurosci.* **16**, 6634 (1996).
12. J. A. Dzubay, C. E. Jahr, *J. Neurosci.* **19**, 5265 (1999).
13. M. Iino, S. Ozawa, K. Tsuzuki, *J. Physiol.* **424**, 151 (1990).
14. S. Ozawa, M. Iino, K. Tsuzuki, *J. Neurophysiol.* **66**, 2 (1991).
15. T. Isa, S. Itazawa, M. Iino, K. Tsuzuki, S. Ozawa, *J. Physiol.* **491**, 719 (1996).
16. J. Grosche *et al.*, *Nature Neurosci.* **2**, 139 (1999).
17. Quantitative evaluation of the morphological changes is available in the supplementary information on *Science* Online at www.sciencemag.org/cgi/content/full/292/5518/926/DC1.
18. F. A. Chaudhry *et al.*, *Neuron* **15**, 711 (1995).
19. K. Yamada *et al.*, *J. Comp. Neurol.* **418**, 106 (2000).
20. B. Barbour, B. U. Keller, I. Llano, A. Marty, *Neuron* **12**, 1331 (1994).
21. C. Auger, D. Attwell, *Neuron* **28**, 547 (2000).
22. J. Mariani, J.-P. Changeux, *J. Neurosci.* **1**, 696 (1981).

8 January 2001; accepted 20 March 2001

Integrated Genomic and Proteomic Analyses of a Systematically Perturbed Metabolic Network

Trey Ideker,[1,2]* Vesteinn Thorsson,[1,2] Jeffrey A. Ranish,[1,2] Rowan Christmas,[1] Jeremy Buhler,[3] Jimmy K. Eng,[1] Roger Bumgarner,[4] David R. Goodlett,[1] Ruedi Aebersold,[1,2] Leroy Hood[1,2]

We demonstrate an integrated approach to build, test, and refine a model of a cellular pathway, in which perturbations to critical pathway components are analyzed using DNA microarrays, quantitative proteomics, and databases of known physical interactions. Using this approach, we identify 997 messenger RNAs responding to 20 systematic perturbations of the yeast galactose-utilization pathway, provide evidence that approximately 15 of 289 detected proteins are regulated posttranscriptionally, and identify explicit physical interactions governing the cellular response to each perturbation. We refine the model through further iterations of perturbation and global measurements, suggesting hypotheses about the regulation of galactose utilization and physical interactions between this and a variety of other metabolic pathways.

For organisms with fully sequenced genomes, DNA microarrays are an extremely powerful technology for measuring the mRNA expression responses of practically every gene (*1*). Technologies for globally and quantitatively measuring protein expression are also becoming feasible (*2*), and developments such as the two-hybrid system are enabling construction of a map of interactions among proteins (*3*). Although such large-scale data have proven invaluable for distinguishing cell types and biological states, new approaches are needed which, by integrating these diverse data types and assimilating them into biological models, can predict cellular behaviors that can be tested experimentally. We propose and apply one such strategy here, consisting of four distinct steps:

(i) Define all of the genes in the genome and the subset of genes, proteins, and other small molecules constituting the pathway of interest. If possible, define an initial model of the molecular interactions governing pathway function, drawn from previous genetic and biochemical research.

(ii) Perturb each pathway component through a series of genetic (e.g., gene deletions or overexpressions) or environmental (e.g., changes in growth conditions or temperature) manipulations. Detect and quantify the corresponding global cellular response to each perturbation with technologies for large-scale mRNA- and protein-expression measurement.

(iii) Integrate the observed mRNA and protein responses with the current, pathway-specific model and with the global network of protein-protein, protein-DNA, and other known physical interactions.

(iv) Formulate new hypotheses to explain

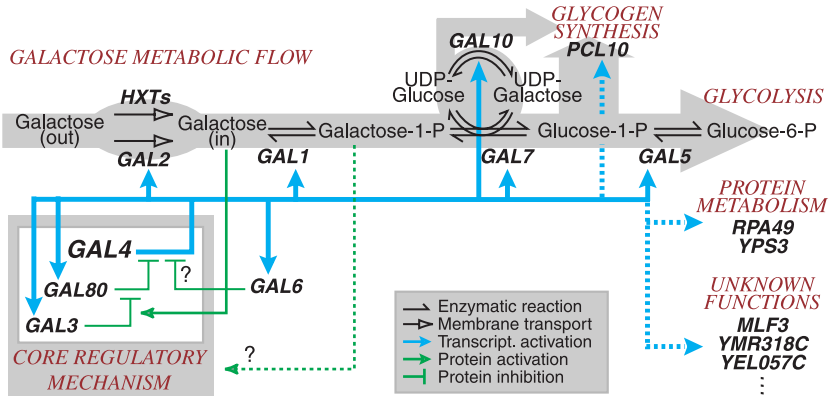

Fig. 1. Model of galactose utilization. Yeast metabolize galactose through a series of steps involving the *GAL2* transporter and enzymes produced by *GAL1*, *GAL7*, *GAL10*, and *GAL5*. These genes are transcriptionally regulated by a mechanism consisting primarily of *GAL4*, *GAL80*, and *GAL3*. *GAL6* produces another regulatory factor thought to repress the GAL enzymes in a manner similar to *GAL80*. Dotted interactions denote model refinements supported by this study.

[1]The Institute for Systems Biology, 4225 Roosevelt Way NE, Suite 200, Seattle, WA 98105, USA. Departments of [2]Molecular Biotechnology, [3]Computer Science, and [4]Microbiology, University of Washington, Seattle, WA 98195, USA.

*To whom correspondence should be addressed at The Institute for Systems Biology. E-mail: tideker@systemsbiology.org

observations not predicted by the model. Design additional perturbation experiments to test these, and iteratively repeat steps (ii), (iii), and (iv).

As proof-of-principle, we now implement this integrated approach to explore the process of galactose utilization (GAL) in the yeast *Saccharomyces cerevisiae*. The GAL pathway is a classic example of a genetic regulatory switch, in which enzymes required specifically for transport and catabolism of galactose are expressed only when galactose is present and repressing sugars such as glucose are absent. Extensive biochemical studies (*4*) and saturating mutant screens (*5*) have defined the genes, gene products, and metabolic substrates required for function of this process and have elucidated the key molecular interactions that lead to pathway activation or inhibition. Thus, by combining this prior work with the complete sequence of the yeast genome, step (i) above has in large part already been accomplished. In steps (ii) through (iv) that follow, we report the first large-scale comparison of mRNA and protein responses, describe an ongoing attempt to systematically explain these responses using existing databases of regulatory and other physical interactions, and explore a number of refinements to the GAL model suggested by these integrative studies.

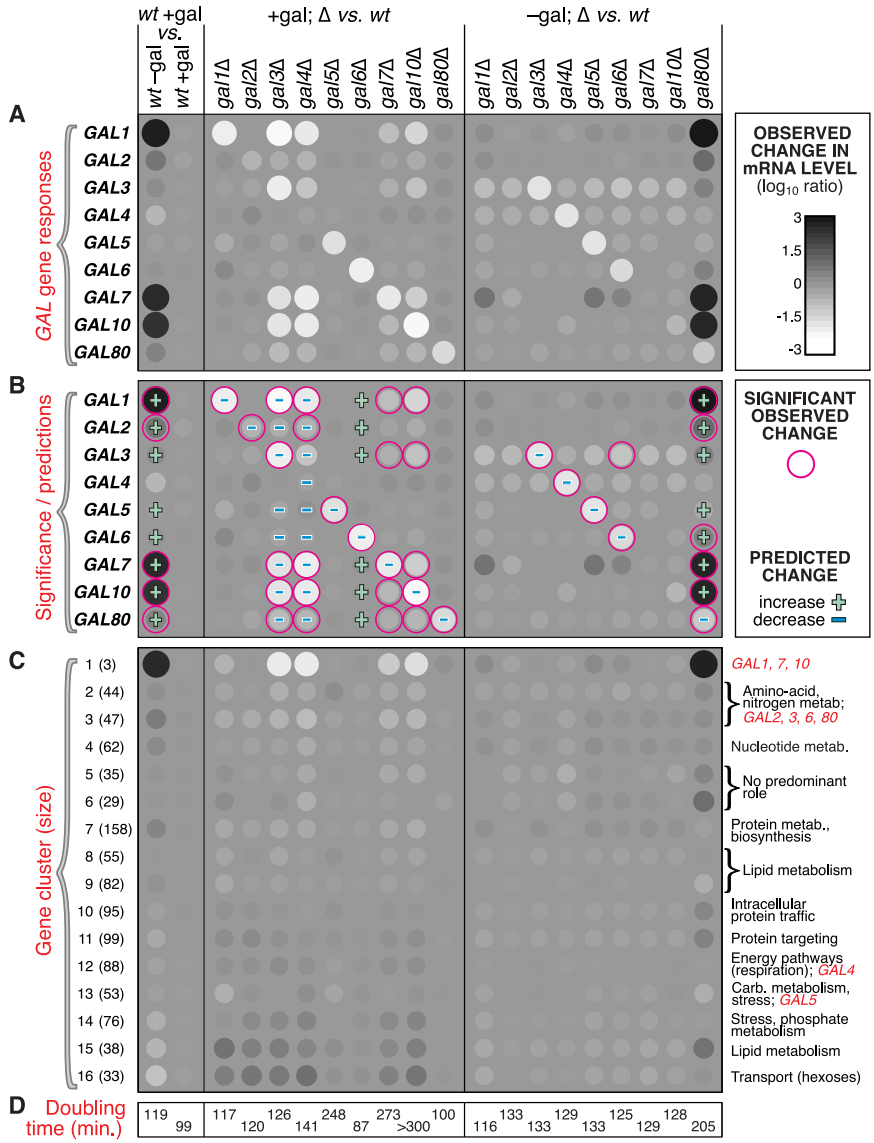

Fig. 2. Perturbation matrix. Microarrays were used to measure the mRNA expression profiles of yeast growing under each of 20 perturbations to the GAL pathway. (**A**) Each spot represents the change in expression of a GAL gene due to a particular perturbation (listed above each column); medium gray (i.e., the same level as figure background) represents no change, whereas darker or lighter shades represent increased or reduced expression, respectively. The left half of the matrix shows expression changes for each deletion strain as compared to *wt*, with both strains grown in the presence of galactose; the right half shows the same differential comparison, but with both strains grown in the absence of galactose (*35*). The *wt*+gal versus *wt*–gal perturbation (far left) isolates the effects of growth with and without galactose, whereas the *wt*+gal versus *wt*+gal perturbation (second from left) serves as a negative control. (**B**) Expression profiles as in (A), with significant changes ($\lambda \geq 45$) circled in magenta. Also superimposed are the qualitative changes (+/−) that we expect using the Fig. 1 model [see Step (iv)]. (**C**) Average expression profiles for genes in each of 16 clusters. Clusters contained genes involved in a variety of metabolic processes, as well as genes of unknown function [Web table 1 (*20*)]; particular Biological Processes [Gene Ontology Database, March 2001 (*36*)] occurring at higher-than-expected frequencies within each cluster are annotated at right. (**D**) Cellular doubling time in each of the 20 conditions, measured before harvest.

Step (i): As shown in Fig. 1, galactose utilization consists of a biochemical pathway that converts galactose into glucose-6-phosphate and a regulatory mechanism that controls whether the pathway is on or off. This process has been reviewed extensively (*4, 6*) and involves at least three types of proteins. A transporter gene (*GAL2*) encodes a permease that transports galactose into the cell; several other hexose transporters (HXTs) may also have this ability (*7*). A group of enzymatic genes encodes the proteins required for conversion of intracellular galactose, including galactokinase (*GAL1*), uridylyltransferase (*GAL7*), epimerase (*GAL10*), and phosphoglucomutase (*GAL5*/*PGM2*). The regulatory genes *GAL3*, *GAL4*, and *GAL80* exert tight transcriptional control over the transporter, the enzymes, and to a certain extent, each other. GAL4p is a DNA-binding factor that can strongly activate transcription, but in the absence of galactose, GAL80p binds GAL4p and inhibits its activity. When galactose is present in the cell, it causes GAL3p to associate with GAL80p. This association causes GAL80p to release its repression of GAL4p, so that the transporter and enzymes are expressed at a high level.

Although these genes and interactions form the core of the GAL pathway, the complete regulatory mechanism is more complex (*8–11*) and involves genes whose roles in galactose utilization are not entirely clear (*12, 13*). For instance, the gene *GAL6* (*LAP3*) functions predominantly in a drug-resistance pathway, but can suppress transcription of the GAL transporter and enzymes under certain conditions and may itself be transcriptionally controlled by *GAL4* (*14*).

Step (ii): Guided by the current model, we applied 20 initial perturbations to the GAL pathway. Wild-type (*wt*) and nine genetically altered yeast strains were examined (*15*), each with a complete deletion of one of the nine GAL genes: transport (*gal2*Δ), enzymatic (*gal1*Δ, *gal5*Δ, *gal7*Δ, or *gal10*Δ), or regulatory (*gal3*Δ, *gal4*Δ, *gal6*Δ, or *gal80*Δ). These strains were perturbed environmentally by growth in the presence (+gal) or absence (–gal) of 2% galactose, with 2% raffinose provided in both media (*16*).

We examined global changes in mRNA

expression resulting from each perturbation, with DNA microarrays of approximately 6200 nuclear yeast genes as described (*17*). In each experiment, fluorescently labeled cDNA from a perturbed strain was hybridized against labeled cDNA from a reference strain (*wt*, grown in +gal media). To obtain robust estimates of fluorescent intensity, four replicate hybridizations were performed for each perturbation. Using a statistical method based on maximum-likelihood estimation (*18*), we identified 997 genes whose mRNA levels differed significantly from reference under one or more perturbations. This set was then divided into 16 clusters using self-organizing maps (*19*), where each cluster contained genes with similar expression responses over all perturbations. Figure 2 displays a matrix summarizing the effects of perturbation on mRNA expression of the GAL genes and gene clusters [complete data provided in Web table 1 (*20*)].

Are the observed changes in mRNA expression also reflected at the level of protein abundance? To address this question, we examined differences in protein abundance between *wt*+gal and *wt*–gal conditions using isotope-coded affinity tag (ICAT) reagents and tandem mass spectrometry (MS/MS) (*21*). Equal amounts of protein extracts from *wt*+gal and *wt*–gal cultures were labeled with isotopically heavy and normal ICAT reagents, respectively, then combined and digested with trypsin. The resulting peptide mixture was fractionated by multidimensional chromatography and analyzed by MS/MS. Computational analysis of the tandem mass spectra was used to identify the proteins from which specific peptides originated and to indicate relative abundances of the heavy and normal ICAT isotopes of each of these peptides.

We obtained protein-abundance ratios for a total of 289 proteins [Web table 1 (*20*)], including all of the GAL enzymes and the transporter. Figure 3 shows protein-abundance ratios versus the corresponding mRNA-expression ratios obtained with DNA microarrays: as a whole, protein-abundance ratios were moderately correlated with their mRNA counterparts ($r = 0.61$, $P < 1.3 \times 10^{-20}$). Although approximately 30 proteins displayed clear changes in abundance between the *wt*+gal and *wt*–gal conditions ($|\log_{10}$ ratio$| > 0.25$), mRNA levels for 15 of these did not change significantly in response to any perturbation, suggesting that these proteins may be regulated posttranscriptionally. In addition, many ribosomal-protein genes increased three- to fivefold in mRNA but not in protein abundance in response to galactose addition. These results underscore the importance of integrated mRNA- and protein-expression measurements for understanding biological systems.

Step (iii): Can we attribute the observed mRNA and protein changes to underlying regulatory interactions in the cell? Although we already have a model of interactions among the GAL genes, it does not address changes in expression observed for the hundreds of other genes appearing in Figs. 2 and 3. To supplement this model, we assembled a catalog of previously observed physical interactions in yeast by combining a published list of 2709 protein-protein interactions (*3*) with 317 protein→DNA interactions recorded in the transcription-factor databases (*22*). A total of 348 genes associated with interactions in this catalog were affected in mRNA or protein expression by at least one perturbation or involved in two or more interactions with affected genes. Figure 4A displays these genes graphically, along with their 362 associated interactions, as a physical-interaction network.

Genes linked by physical interactions in the network tend to have more strongly correlated expression profiles than genes chosen at random ($P < 0.001$). We believe that these correlations identify network interactions that are likely to have transmitted a change in expression from one gene (or protein) to another over our 20 perturbations. Most straightforwardly, a protein→DNA interaction may be responsible for directly transmitting an expression change from a transcription factor to a highly correlated target gene (e.g., Mcm1→Far1 and Mig1→Fbp1; mRNA expression profile correlations are $r_{Mcm1,Far1} = 0.82$ and $r_{Mig1,Fbp1} = 0.63$). Alternatively, genes A and B may be under control of a common transcription factor C→(A,B): coexpression of A and B provides evidence that C transmits these changes, regardless of whether C itself changes detectably in expression. This is the case for the GAL enzymes regulated by Gal4 (Fig. 4B), amino acid synthesis genes regulated by Gcn4 (Fig. 4C), and a class of gluconeogenic genes controlled by Sip4 (Sip4→Fbp1, Pck1, Icl1). Finally, we may scan the network for indirect effects, such as a change in A transmitted to B through a protein-protein interaction with a signaling protein (e.g., Gcr2–Gcr1→Tpi1; $r_{Gcr2,Tpi1} = -0.86$). Many other physically interacting, strongly correlated genes are listed in Web table 2 (*20*); each of these associates an observed change in gene expression with the regulatory interaction(s) likely to have caused it.

Ultimately, we wish to determine paths through the network connecting perturbed GAL genes to every other affected gene. This is not always possible, because many of the required interactions linking galactose utilization to other metabolic processes are still unknown. However, analysis of our expression data suggests that Gal4p directly regulates genes in several of these processes through novel protein→DNA interactions. To identify putative interactions, we looked for the well-characterized Gal4p-binding site (*23*) upstream of genes in expression clusters 1, 2, and 3, which together contained all seven genes with established Gal4p-binding sites. Of the 87 remaining genes in these three clusters, nine had Gal4p-binding sites not previously identified [Web table 3 (*20*)], a significantly greater proportion than were

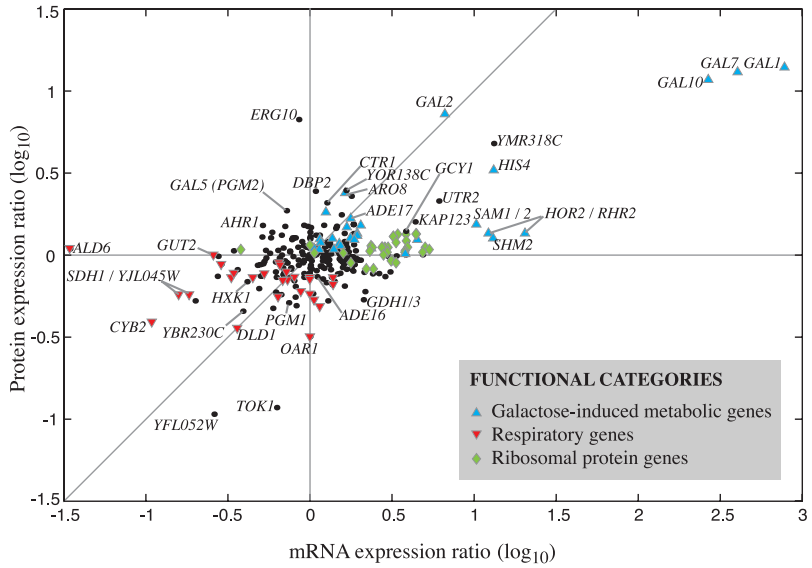

Fig. 3. Scatter plot of protein expression versus mRNA expression ratios. Ratios of *wt*+gal to *wt*−gal protein expression, measured for each of 289 genes using the ICAT technique, are plotted against the corresponding mRNA expression ratios measured by microarray. Many genes with elevated mRNA or protein expression in *wt*+gal were metabolic (▲) or ribosomal (◆), whereas genes involved in respiration (▼) almost always had reduced expression levels. Names of genes that were indistinguishable in both mRNA and protein (due to high sequence similarity) are separated by a slash.

found in clusters 4 through 16 (10.3% versus 2.8%; $P < 0.002$). This set of nine contained genes involved in glycogen accumulation and protein metabolism as well as several genes of unknown function (e.g., *YMR318C*, a gene shown in Fig. 3 to have strong mRNA and protein responses to galactose induction) (*24*). As shown in Fig. 1, we suggest that Gal4p may regulate these genes by direct binding.

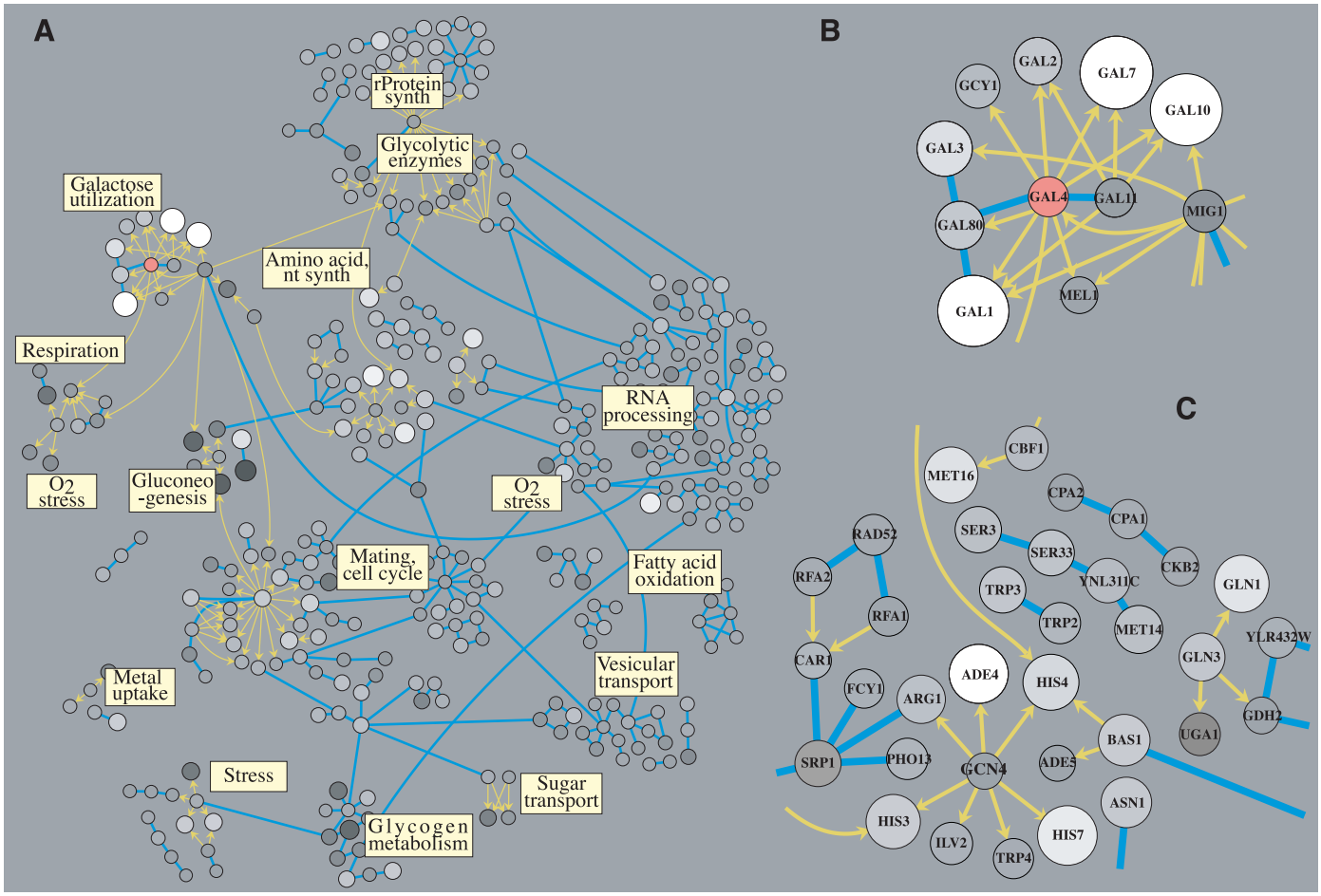

Fig. 4. Integrated physical-interaction network. Nodes represent genes, a yellow arrow directed from one node to another signifies that the protein encoded by the first gene can influence the transcription of the second by DNA binding (protein→DNA), and a blue line between two nodes signifies that the corresponding proteins can physically interact (protein-protein). Highly interconnected groups of genes tend to have common biological function and are labeled accordingly. (**A**) Effects of the *gal4*Δ+gal perturbation are superimposed on the network, with *GAL4* colored red and the gray scale intensity of other nodes representing changes in mRNA as in Fig. 2 (node diameter also scales with the magnitude of change). Regions corresponding to (**B**) galactose utilization and (**C**) amino acid synthesis are detailed at right. Graphical layout and network display were performed automatically using software based on the *LEDA* toolbox (*37*). An enlarged version of (A) is provided in (*20*).

Fig. 5. Tree comparing gene-expression changes resulting from different perturbations to the GAL pathway. We used the *Neighbor* and *Drawtree* programs (*38*) to construct a hierarchical-clustering tree (*39*) based on Euclidean distance between perturbation profiles, where each profile consists of $\log_{10}$ mRNA expression ratios over the set of 997 significantly affected genes. The closer two perturbations are to each other through the branches of the tree, the more similar their observed changes in gene expression. Leaves of the tree are labeled with the relevant genetic perturbation (wild-type or gene deletion) followed by the environmental perturbation (+/– gal). Twenty initial perturbations (solid branches) and three follow-up perturbations are shown (dotted branches). As in Fig. 2, profiles for all genetic perturbations are relative to that of the wild type, with both strains grown in identical media (+gal or –gal).

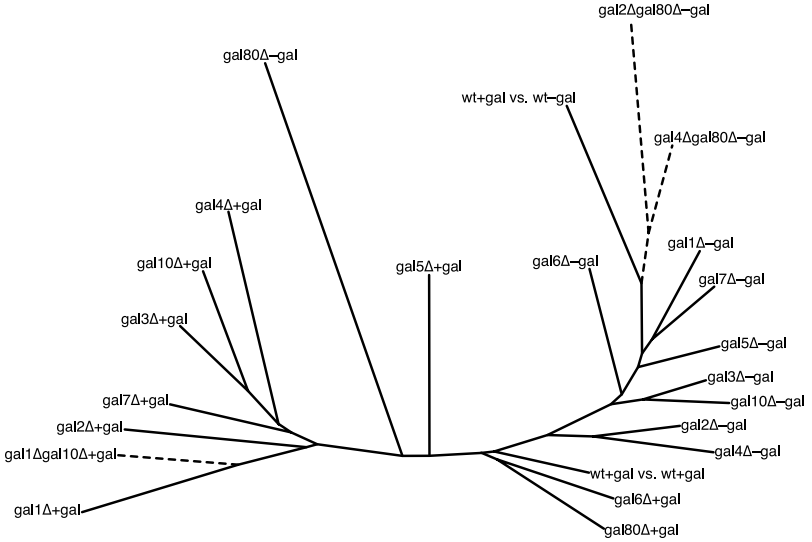

Step (iv): Lastly, how do the observed responses of GAL genes compare to their predicted behavior? Figure 2B shows the qualitative changes (+ and –) in mRNA expression that we predicted based on the model shown in Fig. 1 and from current knowledge of galactose utilization as summarized in Step (i). In general, these were in good agreement with the observed changes. For example, growth of wild-type cells in +gal versus –gal media significantly induced *GAL1*, *GAL2*, *GAL7*, *GAL10*, and *GAL80* as expected, while deleting the positive regulators *GAL3* and *GAL4* led to a significant expression decrease in many of these genes. In –gal media, deletion of the repressor *GAL80* caused a dramatic increase in GAL-enzyme expression; in +gal, this deletion had little or no effect on these genes, presumably because they were already highly expressed.

A number of observations were not predicted by the model and are listed in Web table 4 (*20*); in many cases, these suggest new regulatory phenomena that may be tested by hypothesis-driven approaches. For example, in the presence of galactose, *gal7* and *gal10* deletions unexpectedly reduced the expression levels of other GAL enzymes. Because the metabolite Gal-1-P is known to accumulate in cells lacking functional Gal7 and is detrimental in large quantities (*25*), one hypothesis is that the observed expression-level changes are dependent on build-up of Gal-1-P or one of its metabolic derivatives. Under this model, the cell would limit metabolite accumulation by first sensing toxic levels through an unknown mechanism, then triggering a decrease in GAL-enzyme expression (Fig. 1). Alternative scenarios are also possible, such as a model in which *GAL10* influences the expression of *GAL7* and *GAL1* through transcriptional interference within the *GAL1-10-7* locus (*9*).

To test the hypothesis that the effects of *gal7*Δ and *gal10*Δ are dependent on increased levels of Gal-1-P or a derivative molecule, we examined the expression profile of a *gal1*Δ*gal10*Δ double deletion growing in +gal conditions (relative to the *wt*+gal reference). We predicted that in this strain, the absence of *GAL1* activity would prevent build-up of Gal-1-P and the changes in GAL gene expression would not occur. Conversely, if the expression changes did not depend on Gal-1-P (e.g., are caused by chromosomal interactions at the *GAL1-10-7* locus), they would also be likely to occur in the *gal1*Δ*gal10*Δ strain. Consistent with our initial hypothesis, GAL-enzyme expression was not significantly affected by this perturbation, and as shown in Fig. 5, the expression profile of *gal1*Δ*gal10*Δ over all affected genes was more similar to the profile of *gal1*Δ+gal than to that of *gal10*Δ+gal or any other perturbation.

Another unanticipated observation was the slow growth of the *gal80*Δ mutant in –gal conditions (Fig. 2D), the large number of gene clusters affected by this perturbation (Fig. 2C, compare rightmost column to the other eight columns in the –gal set), and the corresponding large distance between the *gal80*Δ–gal expression profile and every other profile in Fig. 5. Since this perturbation leads to constitutive expression of the GAL enzymes and transporter, we wished to determine whether the widespread expression changes were dependent on these genes. Accordingly, we measured the expression profile of a *gal4*Δ*gal80*Δ–gal double deletion, in which the GAL enzymes and transporter are not expressed. Both the doubling time (144 min) and overall expression profile of this strain (Fig. 5) were more similar to those of *gal4*Δ (129 min) than *gal80*Δ (205 min), suggesting that the effects of the *gal80*Δ perturbation are indeed mediated by other GAL genes. To further determine which GAL genes were important for the effect, we measured the expression profile of a *gal2*Δ*gal80*Δ–gal perturbation, in which the GAL transporter was absent. This profile was more similar to that of *gal2*Δ than *gal80*Δ, providing evidence that the transporter is necessary to produce the slow growth and expression changes seen for the *gal80*Δ perturbation.

We expect that more directed experimental approaches (i.e., biochemistry, genetics, cell biology) will be required to test these ideas and further deepen our understanding of galactose utilization and its interacting networks. Even so, global and integrated analyses are extremely powerful for suggesting new hypotheses, especially with regard to the regulation of a pathway and its interconnections with other pathways. As technologies for cellular perturbation and global measurement mature, these approaches will soon become feasible in higher eukaryotes.

References and Notes

1. E. S. Lander, *Nature Genet.* **21**, 3 (1999).
2. S. P. Gygi *et al.*, *Nature Biotechnol.* **17**, 994 (1999).
3. B. Schwikowski, P. Uetz, S. Fields, *Nature Biotechnol.* **18**, 1257 (2000). [www.nature.com/nbt/web_extras/supp_info/nbt1200_1257/]
4. D. Lohr, P. Venkov, J. Zlatanova, *FASEB J.* **9**, 777 (1995).
5. H. C. Douglas, D. C. Hawthorne, *Genetics* **49**, 837 (1964).
6. R. J. Reece, *Cell Mol. Life Sci.* **57**, 1161 (2000).
7. R. Wieczorke *et al.*, *FEBS Lett.* **464**, 123 (1999).
8. M. Johnston, J. S. Flick, T. Pexton, *Mol. Cell. Biol.* **14**, 3834 (1994).
9. I. H. Greger, N. J. Proudfoot, *EMBO J.* **17**, 4771 (1998).
10. G. Peng, J. E. Hopper, *Mol. Cell. Biol.* **20**, 5140 (2000).
11. J. R. Rohde, J. Trinh, I. Sadowski, *Mol. Cell. Biol.* **20**, 3880 (2000).
12. S. Rudoni, I. Mauri, M. Ceriani, P. Coccetti, E. Martegani, *Int. J. Biochem. Cell Biol.* **32**, 215 (2000).
13. L. Fu, A. Miseta, D. Hunton, R. B. Marchase, D. M. Bedwell, *J. Biol. Chem.* **275**, 5431 (2000).
14. W. Zheng, H. E. Xu, S. A. Johnston, *J. Biol. Chem.* **272**, 30350 (1997).
15. Strains were derived from the wild-type haploid MATa strain BY4741 (ATCC #201388, MATa *his3*Δ*1 leu2*Δ*0 met15*Δ*0 ura3*Δ*0*). The mutants *gal1*Δ, *gal3*Δ, *gal5*Δ, *gal7*Δ, and *gal10*Δ were constructed by complete replacement of the corresponding genes with kanR using the loxP-kanR-loxP cassette (*26*), while *gal2*Δ, *gal4*Δ, *gal6*Δ, and *gal80*Δ were obtained from the Saccharomyces Genome Deletion Project (*27*) and were constructed analogously. Strains *gal2*Δ*gal80*Δ and *gal4*Δ*gal80*Δ were obtained by mating and sporulation of the single-deletion mutants; *gal1*Δ*gal10*Δ (#R4146) was a generous gift from C. Roberts of Rosetta Inpharmatics.
16. Yeast were inoculated in 100 ml of either GAL-inducing "+gal" media (1% yeast extract, 2% peptone, 2% raffinose, 2% galactose) or noninducing "–gal" media (1% yeast extract, 2% peptone, 2% raffinose). Cultures were grown overnight at 30°C to a density of 1 to 2 OD_{600}, washed in 5 ml H_2O, and snap-frozen.
17. T. Ideker, V. Thorsson, A. Siegel, L. Hood, *J. Computational Biol.* **7**, 805 (2001). [www.systemsbiology.org/VERAandSAM/]
18. A likelihood statistic λ was computed for each gene to determine whether its mRNA expression level differed between the two cell populations compared by a microarray (*17*); genes having $\lambda \geq 45$ were selected as differentially expressed. This value was approximately the maximum obtained in control experiments in which the two mRNA populations were derived from identical strains and growth conditions (*wt*+gal).
19. The 997 affected genes were clustered based on Euclidean distance between their $\log_{10}$ expression ratios over all perturbation conditions, using a 4 row by 4 column self-organizing map (SOM) implemented by the *GeneCluster* application (*28*), with 100 epochs.
20. Supplementary material is available at www.sciencemag.org/cgi/content/full/292/5518/929/DC1
21. Cells were grown and harvested as for mRNA measurement, with proteins extracted according to Futcher (*29*). Extracts were desalted (Biorad 10DG columns) in 50 mM tris 8.3, 1 mM EDTA, and 0.05% SDS. The ICAT method (*2*) was applied to 300 μg of protein from each extract, with the following modifications. After trypsin digestion, peptides were fractionated on a 2.1 mm by 200 mm polySULFOETHYL A column (PolyLC) by running a salt gradient from 0 to 25% Buffer B (5 mM KH_2PO_4, pH 3.0, 350 mM KCl, 25% CH_3CN) over 30 min, followed by 25 to 100% Buffer B over 20 min at 0.2 ml/min. Labeled peptides were isolated from each cation-exchange-chromatography fraction by monomeric avidin (Pierce) affinity chromatography. Then, 10 to 80% of the peptide mixture was analyzed by capillary-liquid-chromatography MS/MS.
22. Protein-protein interactions, as reported in (*3*), were derived predominantly through two-hybrid assays and interactions culled from the literature. Protein-DNA interactions were obtained with permission from TRANSFAC (*30*) and SCPD (*31*) and represent all interactions in these databases as of July 2000. A more comprehensive analysis of the physical-interaction network will be provided in a future publication.
23. A nucleotide weight matrix model of the binding site (TRANSFAC site matrix M00049) was used to identify potential binding sites in the promoter regions of genes in the 997-gene set. Nucleotide sequences of up to 800 bp upstream of translation start sites, terminating at the nearest upstream ORFs, were scored against the weight matrix using MatInspector (*32*) with core similarity 0.7 and matrix similarity 0.8.
24. While this work was in review, one of these genes (*PCL10*) was identified as a target of Gal4p by direct DNA-binding assay (*33*). Also, *YMR318C* was implicated in a previous binding-site prediction study (*34*).
25. K. Lai, L. J. Elsas, *Biochem. Biophys. Res. Commun.* **271**, 392 (2000).
26. U. Guldener, S. Heck, T. Fielder, J. Beinhauer, J. H. Hegemann, *Nucleic Acids Res.* **24**, 2519 (1996).
27. E. A. Winzeler *et al.*, *Science* **285**, 901 (1999).
28. P. Tamayo *et al.*, *Proc. Natl. Acad. Sci. U.S.A.* **96**, 2907 (1999).
29. B. Futcher, G. I. Latter, P. Monardo, C. S. McLaughlin, J. I. Garrels, *Mol. Cell Biol.* **19**, 7357 (1999).
30. E. Wingender *et al.*, *Nucleic Acids Res.* **28**, 316 (2000). [http://transfac.gbf.de/TRANSFAC/]
31. J. Zhu, M. Q. Zhang, *Bioinformatics* **15**, 607 (1999). [http://cgsigma.cshl.org/jian/]
32. K. Quandt, K. Frech, H. Karas, E. Wingender, T. Werner, *Nucleic Acids Res.* **23**, 4878 (1995).
33. B. Ren *et al.*, *Science* **290**, 2306 (2000).

34. F. P. Roth, J. D. Hughes, P. W. Estep, G. M. Church, *Nature Biotechnol.* **16**, 939 (1998).
35. In Fig. 2, deletion strains grown in − gal are displayed relative to *wt*–gal conditions by subtracting the $\log_{10}$ expression ratio of *wt*–gal versus reference from the $\log_{10}$ expression ratio of the deletion strain versus reference. As predicted and confirmed experimentally (T. Ideker, V. Thorsson, data not shown), this operation results in approximately a $\sqrt{2}$-fold increase in error.
36. M. Ashburner *et al.*, *Nature Genet.* **25**, 25 (2000). [www.geneontology.org/]
37. K. Mehlhorn, S. Naeher, *The LEDA Platform of Combinatorial and Geometric Computing* (Cambridge Univ. Press, Cambridge, 1999). [www.algorithmic-solutions.com/]
38. J. Felsenstein, *Cladistics* **5**, 164 (1989).
39. M. B. Eisen, P. T. Spellman, P. O. Brown, D. Botstein, *Proc. Natl. Acad. Sci. U.S.A.* **95**, 14863 (1998).
40. We thank G. van den Engh for ideas on visual display; B. Schwikowski and P. Uetz for early access to protein interactions; A. Siegel, K. Y. Yeung, E. Cho, Q. Zong, and E. Yi for assistance with global analysis; T. Young, D. Morris, K. Dimitrov, M. Johnston, and I. Sadowski for informative discussions; and J. Hopper, J. Aitchison, and L. Kruglyak for critical reading of the manuscript. This work was funded by grants from NIH (T.I., J.A.R., R.A.) and the Sloan Foundation/U.S. Department of Energy (V.T.).

5 October 2000; accepted 5 April 2001

Vital Involvement of a Natural Killer Cell Activation Receptor in Resistance to Viral Infection

Michael G. Brown,[1]*† Ayotunde O. Dokun,[1,2]* Jonathan W. Heusel,[1] Hamish R. C. Smith,[1] Diana L. Beckman,[1] Erika A. Blattenberger,[1] Chad E. Dubbelde,[1] Laurie R. Stone,[1] Anthony A. Scalzo,[3] Wayne M. Yokoyama[1]‡

Natural killer (NK) cells are lymphocytes that can be distinguished from T and B cells through their involvement in innate immunity and their lack of rearranged antigen receptors. Although NK cells and their receptors were initially characterized in terms of tumor killing in vitro, we have determined that the NK cell activation receptor, Ly-49H, is critically involved in resistance to murine cytomegalovirus in vivo. Ly-49H requires an immunoreceptor tyrosine-based activation motif (ITAM)–containing transmembrane molecule for expression and signal transduction. Thus, NK cells use receptors functionally resembling ITAM-coupled T and B cell antigen receptors to provide vital innate host defense.

Natural killer (NK) cells were first identified because of their "natural" ability to kill tumors in vitro, an ability that is now known to occur through activation receptors that trigger the release of perforin-containing cytolytic granules [reviewed in (*1*)]. These lymphocytes can be distinguished from T and B cells because they do not express rearranged antigen receptors and are not directly involved in acquired immunity. However, NK cells participate in early innate host defense against pathogens and are generally thought to counter infections through a nonspecific response to inflammatory cytokines that induce their production of interferon-γ (*2*). Yet, NK cells appear to respond specifically against certain pathogens. For example, in humans, selective NK cell deficiency is associated with recurrent systemic infections, especially with herpesviruses such as cytomegalovirus (*3*). This is closely paralleled by the susceptibility of NK cell–depleted mice to murine cytomegalovirus (MCMV) but not to lymphocytic choriomeningitis virus (*4*). Although the mechanisms underlying this susceptibility are incompletely understood, NK cell receptors that activate tumor cytotoxicity may play important roles in innate defense against specific infections (*5*).

The critical involvement of NK cell activation receptors in defense against pathogens is highlighted by the expression of virus-encoded proteins that interfere with natural killing (*6*). In many cases, these proteins enhance the function of inhibitory major histocompatibility complex (MHC) class I–specific NK cell receptors that potentially interfere with signals from activation receptors, such as Ly-49D and Ly-49H, that are coupled to immunoreceptor tyrosine-based activation motif (ITAM)–containing transmembrane

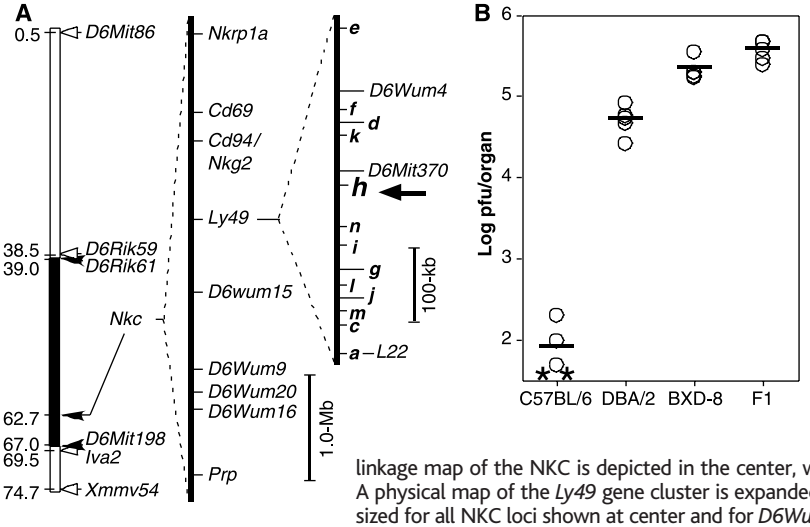

Fig 1. BXD-8 mice possess the NKC^{B6} haplotype and display MCMV susceptibility that is not complemented by DBA/2. (**A**) Genetic and physical maps of NKC-linked loci on mouse chromosome 6. A genetic linkage map and schematic diagram of the BXD-8 chimeric chromosome 6 is represented at left, based on the Mouse Genome Informatics database (*14*, *25*). Chromosomal regions derived from the C57BL/6 (solid bar) or DBA/2 (open bars) inbred progenitor strains are indicated, along with genetic position (distance is indicated in centimorgans from the centromere) of C57BL/6 alleles (solid arrowheads) and DBA/2 (open arrowheads) alleles for the recombination breakpoints. Sequence-tagged site markers that reside close to the centromere and telomere are also shown. Thus far, in BXD-8, all loci reported to reside between *D6Mit86* and *D6Rik59* (36 tested loci) and between *Iva2* and *Xmmv54* (10 loci) contain DBA/2 alleles. C57BL/6 alleles account for all BXD-8 loci reported to reside between *D6Rik61* and *D6Mit198*, except for the *Cmv1* locus (*9*, *25*). A physical linkage map of the NKC is depicted in the center, with selected loci that have been useful to distinguish alleles (*19*). A physical map of the *Ly49* gene cluster is expanded at right (*26*, *27*). BXD-8 and C57BL/6 NKC alleles are identically sized for all NKC loci shown at center and for *D6Wum4*, *D6Mit370*, *Ly49g*, and *Ly49a* (*L22*). Surrounding *Ly49h* are the *Ly49k* and *Ly49n* pseudogenes (*28*). (**B**) MCMV replication in F_1 hybrid offspring from DBA/2 and BXD-8. Three days after infection [with MCMV Smith strain, 2×10^4 plaque-forming units (PFUs)], organ viral titers were assessed in tissue homogenates collected from C57BL/6, DBA/2, BXD-8, and (DBA/2 × BXD-8) F_1 hybrid mice (five mice per group), as indicated. Spleen titers are shown here; liver titers are available online (*8*). Each point represents the average titer determined for an individual mouse. In the spleens of two C57BL/6-infected mice, viral replication was below the level of detection by this assay and is indicated with asterisks. Mean viral titers for each group are depicted as horizontal bars. For mice with titers below the level of detection of the assay, the minimum number of detectable PFUs (10^2) was assumed to determine the mean. This assumption overestimates the mean for the group having titers below detectable levels.